

# Quasielastic ${}^3\text{He}(\vec{e}, e')$ Asymmetry in the Threshold Region

M. Nycz,<sup>1,\*</sup> W. Armstrong,<sup>2</sup> T. Averett,<sup>3</sup> C. Ayerbe Gayoso,<sup>3</sup> X. Bai,<sup>1</sup> J. Bane,<sup>4</sup> S. Barcus,<sup>5</sup> J. Benesch,<sup>5</sup> H. Bhatt,<sup>6</sup> D. Bhetuwal,<sup>6</sup> D. Biswas,<sup>7</sup> A. Camsonne,<sup>5</sup> G. Cates,<sup>1</sup> J-P. Chen,<sup>5</sup> J. Chen,<sup>3</sup> M. Chen,<sup>1</sup> C. Cotton,<sup>1</sup> M-M. Dalton,<sup>5</sup> A. Deltuva,<sup>8</sup> A. Deur,<sup>5</sup> B. Dhital,<sup>9</sup> B. Duran,<sup>10</sup> S.C. Dusa,<sup>5</sup> I. Fernando,<sup>7</sup> E. Fuchey,<sup>11</sup> B. Gamage,<sup>5</sup> H. Gao,<sup>12</sup> D. Gaskell,<sup>5</sup> T. Gautam,<sup>7</sup> N. Gauthier,<sup>5</sup> J. Golak,<sup>13</sup> J.-O. Hansen,<sup>5</sup> F. Hauenstein,<sup>9</sup> W. Henry,<sup>5</sup> D.W. Higinbotham,<sup>5</sup> G. Huber,<sup>14</sup> C. Jantzi,<sup>1</sup> S. Jia,<sup>10</sup> K. Jin,<sup>1</sup> M. Jones,<sup>5</sup> S. Joosten,<sup>2</sup> A. Karki,<sup>6</sup> B. Karki,<sup>15</sup> S. Katugampola,<sup>1</sup> S. Kay,<sup>14</sup> C. Keppel,<sup>5</sup> E. King,<sup>16</sup> P. King,<sup>15</sup> W. Korsch,<sup>17</sup> V. Kumar,<sup>14</sup> R. Li,<sup>10</sup> S. Li,<sup>18</sup> W. Li,<sup>3</sup> D. Mack,<sup>5</sup> S. Malace,<sup>5</sup> P. Markowitz,<sup>19</sup> J. Matter,<sup>1</sup> M. McCaughan,<sup>5</sup> Z-E. Meziani,<sup>10</sup> R. Michaels,<sup>5</sup> A. Mkrtchyan,<sup>20</sup> H. Mkrtchyan,<sup>20</sup> C. Morean,<sup>4</sup> V. Nelyubin,<sup>1</sup> G. Niculescu,<sup>21</sup> M. Niculescu,<sup>21</sup> C. Peng,<sup>2</sup> S. Premathilake,<sup>1</sup> A. Puckett,<sup>11</sup> A. Rathnayake,<sup>1</sup> M. Rehfuss,<sup>10</sup> P. Reimer,<sup>2</sup> G. Riley,<sup>18</sup> Y. Roblin,<sup>5</sup> J. Roche,<sup>15</sup> M. Roy,<sup>17</sup> P. U. Sauer,<sup>22</sup> S. Scopeta,<sup>23</sup> M. Satnik,<sup>3</sup> B. Sawatzky,<sup>5</sup> S. Seeds,<sup>11</sup> S. S. Širca,<sup>24,25</sup> R. Skibiński,<sup>13</sup> G. Smith,<sup>5</sup> N. Sparveris,<sup>10</sup> H. Szumila-Vance,<sup>5</sup> A. Tadepalli,<sup>5</sup> V. Tadevosyan,<sup>20</sup> Y. Tian,<sup>16</sup> A. Usman,<sup>14</sup> H. Voskanyan,<sup>20</sup> H. Witała,<sup>13</sup> S. Wood,<sup>5</sup> B. Yale,<sup>3</sup> C. Yero,<sup>19</sup> A. Yoon,<sup>26</sup> J. Zhang,<sup>1</sup> Z. Zhao,<sup>12</sup> X. Zheng,<sup>1</sup> and J. Zhou<sup>12</sup>

<sup>1</sup>University of Virginia, Charlottesville, Virginia 22904, USA

<sup>2</sup>Argonne National Laboratory, Lemont, Illinois 60439, USA

<sup>3</sup>William & Mary, Williamsburg, Virginia 23187, USA

<sup>4</sup>University of Tennessee, Knoxville, Tennessee 37996, USA

<sup>5</sup>Thomas Jefferson National Accelerator Facility, Newport News, Virginia 23606, USA

<sup>6</sup>Mississippi State University, Mississippi State, Mississippi 39762, USA

<sup>7</sup>Hampton University, Hampton, Virginia 23669, USA

<sup>8</sup>Institute of Theoretical Physics and Astronomy,

Vilnius University, Saulėtekio al. 3, LT-10257 Vilnius, Lithuania

<sup>9</sup>Old Dominion University, Norfolk, Virginia 23529, USA

<sup>10</sup>Temple University, Philadelphia, Pennsylvania 19122, USA

<sup>11</sup>University of Connecticut, Storrs, Connecticut 06269, USA

<sup>12</sup>Duke University, Durham, North Carolina 27708, USA

<sup>13</sup>Faculty of Physics, Astronomy and Applied Computer Science,  
Jagiellonian University, PL-30348 Kraków, Poland

<sup>14</sup>University of Regina, Regina, Saskatchewan, S4S 0A2 Canada

<sup>15</sup>Ohio University, Athens, Ohio 45701, USA

<sup>16</sup>Syracuse University, Syracuse, New York 13244, USA

<sup>17</sup>University of Kentucky, Lexington, Kentucky 40506, USA

<sup>18</sup>University of New Hampshire, Durham, New Hampshire 03824, USA

<sup>19</sup>Florida International University, Miami, Florida 33199, USA

<sup>20</sup>AANL, 2 Alikhanian Brothers Street, 0036 Yerevan, Armenia

<sup>21</sup>James Madison University, Harrisonburg, VA 22801, USA

<sup>22</sup>Institut für Theoretische Physik, Universität Hannover, D-30167 Hannover, Germany

<sup>23</sup>Dipartimento di Fisica e Geologia, Università degli Studi di Perugia and Istituto Nazionale di Fisica Nucleare,  
Sezione di Perugia, via A. Pascoli, I - 06123 Perugia, Italy

<sup>24</sup>Faculty of Mathematics and Physics, University of Ljubljana, 1000 Ljubljana, Slovenia

<sup>25</sup>Jožef Stefan Institute, 1000 Ljubljana, Slovenia

<sup>26</sup>Christopher Newport University, Newport News, Virginia 23606, USA

(Dated: September 26, 2024)

A measurement of the double-spin asymmetry from electron- ${}^3\text{He}$  scattering in the threshold region of two- and three-body breakup of  ${}^3\text{He}$  was performed at Jefferson Lab, for  $Q^2$  values of 0.1 and 0.2 (GeV/c)<sup>2</sup>. The results of this measurement serve as a stringent test of our understanding of few-body systems. When compared with calculations from plane wave impulse approximation and Faddeev theory, we found that the Faddeev calculations, which use modern nuclear potentials and prescriptions for meson-exchange currents, demonstrate an overall good agreement with data.

As the simplest nuclear environment that involves dynamics beyond the two-nucleon interactions, the  ${}^3\text{He}$

nucleus provides a testing ground of our understanding of the three-nucleon force (3NF), sometimes highlighting flaws or omissions [1]. Significant theoretical effort has been made to accurately characterize three-nucleon systems, including two major methods that describe the process of electron scattering off A=3 nuclei: plane wave

\* mnycz@jlab.org

impulse approximation (PWIA) [2–4] and exact non-relativistic Faddeev calculations [5–9]. The PWIA typically has shown a good agreement with data at large four-momentum transfers. At low four-momentum transfers above the two-body ( $p + d$ ) and three-body ( $p + p + n$ ) breakup threshold, non-relativistic Faddeev calculations that fully include Final State Interactions (FSI) and use realistic nucleon-nucleon potentials along with the Meson Exchange Currents (MEC), have shown a good agreement with data.

Experimental measurements that can directly probe FSI, 3NF, and MEC, would provide additional limits and further refinements to theoretical models. This can be done by identifying kinematic regions where effects due to these three mechanisms are expected to be large. Inclusive unpolarized cross section measurements made in the threshold region showed good agreement with theoretical predictions [10]. On the other hand, initial measurements of spin observables suggested missing elements in theoretical description, possibly due to MEC and FSI, which was improved in later, more precise measurements [11].

We report here a new, precision measurement of the double-spin asymmetry of electron scattering off the  $^3\text{He}$  in the elastic and quasielastic region in the threshold region. In such regions of low momentum transfer, rescattering of the nucleon which interacted with the virtual photon with the remaining nucleons can occur [5], providing a unique testing ground of FSI and MEC. In the following, we describe the formalism, the experiment, data analysis, and the results.

For quasielastic scattering in which longitudinally polarized electrons scattering off a polarized  $^3\text{He}$  target, the inclusive differential cross section can be expressed as [12]:

$$\frac{d\sigma}{d\Omega dE'} = \frac{\alpha^2 \cos^2(\frac{\theta}{2})}{4E^2 \sin^4(\frac{\theta}{2})} \{v_L R_L + v_T R_T - h [v_{T'} \cos\theta^* R_{T'} + 2v_{TL'} \sin\theta^* \cos\phi^* R_{TL'}]\}, \quad (1)$$

where  $\alpha$  is the fine-structure constant,  $E$  is the initial energy,  $\theta$  is the scattered electron angle,  $R_T$  and  $R_L$  are the spin-averaged response functions,  $R_{T'}$  and  $R_{TL'}$  are the spin-dependent response functions, the terms  $v_i$  ( $i = L, T, T', TL'$ ) are kinematic factors, and  $\theta^*$  and  $\phi^*$  are the polar and azimuthal angles of the polarization vector of the nuclear target in the lab frame, with  $\hat{z}$  pointing along the virtual photon momentum,  $\hat{q}$  [13].

The spin-dependent asymmetry is defined as

$$A = \frac{\sigma^{\uparrow\uparrow} - \sigma^{\downarrow\downarrow}}{\sigma^{\uparrow\uparrow} + \sigma^{\downarrow\downarrow}}, \quad (2)$$

where  $\sigma^{\uparrow\uparrow}$  and  $\sigma^{\downarrow\downarrow}$  are the cross section for scattering with the electron spin parallel and anti-parallel to the target spin, respectively. Substituting the expression for the cross section given in Eq.(1) into Eq.(2), the asymmetry can be written as:

$$A = -\frac{\cos\theta^* v_{T'} R_{T'} + 2\sin\theta^* \cos\phi^* v_{TL'} R_{TL'}}{v_L R_L + v_T R_T}. \quad (3)$$

The experiment reported here [13] was performed in Hall C of the Thomas Jefferson National Accelerator Facility (Jefferson Lab) in 2020. The original goal was to determine the first diffractive minima of both electric and magnetic form factors of  $^3\text{He}$  by measuring the double spin asymmetry of  $e-^3\text{He}$  elastic scattering. Meanwhile, the experimental conditions provided an opportunity to also measure the double spin asymmetry of quasielastic scattering. A longitudinally polarized electron beam of 2.2 GeV energy was scattered off a 40-cm long polarized  $^3\text{He}$  target filled to about 12 amagats of density. The beam polarization  $P_b$  was found to be  $(85 \pm 3)\%$ , determined from Moller polarimetry.

Scattered electrons were detected in the Super High Momentum Spectrometer (SHMS). The SHMS consists of five superconducting magnets [14] which follows the form of (DQQQD). The first dipole (D) is a horizontal bender (HB) used to bend scattered electrons by a small angle ( $\approx 3^\circ$ ) and allows the spectrometer to reach a minimum scattering angle of  $5.5^\circ$ . The remaining quadrupole (Q) elements are used for focusing of the scattered particles while the last dipole is used for momentum selection and deflects the particles into the SHMS detectors.

The series of detectors in the SHMS provide position, timing, and particle identification of the scattered particles. The first detector is a pair of drift chambers that provide position and tracking information, which can be coupled with optics properties of the spectrometer to reconstruct the particles scattering angle, momentum, and the interaction position in the target. Following the drift chamber are two planes of hodoscopes, with each plane being comprised of vertical (Y) and horizontal (X) scintillator paddles, and is used primarily as a trigger. A threshold gas Cerenkov detector and an electromagnetic calorimeter are used for particle identification.

The target system included a gaseous polarized  $^3\text{He}$  target, along with an unpolarized reference cell, as well as additional solid targets used for calibration. The  $^3\text{He}$  target was polarized via spin exchange optical pumping [15, 16]. To ascertain the target polarization, a two step process is used. First, the absolute polarization was determined through an Electron Paramagnetic Resonance (EPR) measurement, which served as a calibration point. Second, Adiabatic Fast Passage NMR measurements provide a relative polarization. NMR measurements can be taken more frequently during data collection, and when combined with the calibration constant from the EPR measurement, allows for a determination of the target polarization over time. The target polarization  $P_t$  was found to vary between  $(35 - 45)\%$ , with  $\Delta P_t/P_t = 3\%$ . Two tungsten collimators were placed adjacent to the target cell in order to reduce background events that scattered off the glass windows.

Data were collected at two primary kinematics, which provided asymmetries at four-momentum transfer squares  $Q^2 = 0.1$  and  $Q^2 = 0.2$  ( $\text{GeV}/c$ )<sup>2</sup>. In order to better balance the proportion of elastic and quasielastic events, selected scintillator paddles in the SHMS were

turned off, reducing the acceptance of the spectrometer.

Electrons were identified through particle identification (PID) cuts based on the gas Cerenkov and electromagnetic calorimeter detectors. A minimum response in the Cerenkov of 5 photoelectrons along with an  $E/p$  great than 0.8, where  $E$  is the particle energy measured by the calorimeter and  $p$  is the reconstructed momentum, were required. Additionally, acceptance cuts were used to exclude regions of acceptance not well constrained by the existing optics matrix. Finally, a reconstructed position along the length of the target cell,  $z_{targ}$  was optimized to suppress events which scattered from the glass windows of target cell.

To form the asymmetry, yields were sorted based on the incident electron's helicity:

$$Y^+ = \frac{N^+}{Q^+LT^+} \quad Y^- = \frac{N^-}{Q^-LT^-}, \quad (4)$$

where  $N^+$  ( $N^-$ ) represents the number of detected electrons in  $+$  ( $-$ ) beam helicity state,  $Q^+$  ( $Q^-$ ) and  $LT^+$  ( $LT^-$ ) the corresponding total incident beam charge and the live time, respectively. The asymmetry can then be formed as:

$$A_{raw} = \frac{Y^+ - Y^-}{Y^+ + Y^-}. \quad (5)$$

To determine the acceptance and target cuts, a single-spectrometer Monte Carlo (SIMC) [17] was adapted to describe the experimental setup. To ensure a satisfactory description of the scintillator paddle status, the simulated events were compared with actual data in both the focal plane and the reconstructed target quantities. The simulated events were weighted using elastic and quasielastic cross section models. The individual contributions from elastic and quasielastic scattering as well as the combined distribution were analyzed and showed a good agreement between data and simulation. With the observed good agreement, the momentum distribution was used to separate elastic from the quasielastic spectrum.

The elastic asymmetry extracted from data provided an independent check of the product of the beam and the target polarizations,  $P_b P_t$ . Illustrated in Fig. 1 is the measured elastic asymmetry for the kinematic settings  $Q^2=0.1$  and  $Q^2=0.2$  ( $\text{GeV}/c$ )<sup>2</sup> along with a parameterization [18] for the elastic asymmetry utilizing form factors determined from a sum of Gaussians fits to world data [19]. There is an overall good agreement between the measured asymmetries and predictions at low  $Q^2$ , where the elastic form factors are well constrained, indicating that the product  $P_b P_t$  are reasonably well understood. Due to the limited beam time, however, the  $Q^2$  coverage was not high enough to cover the diffractive minima.

Combining the measured raw asymmetry with the beam and target polarizations, the QE physics asymmetry was obtained as:

$$A_{phys} = \frac{A_{raw}}{P_b P_t} \left( \frac{1}{1 - d_{El}} \right) - A_{El} \left( \frac{d_{El}}{1 - d_{El}} \right), \quad (6)$$

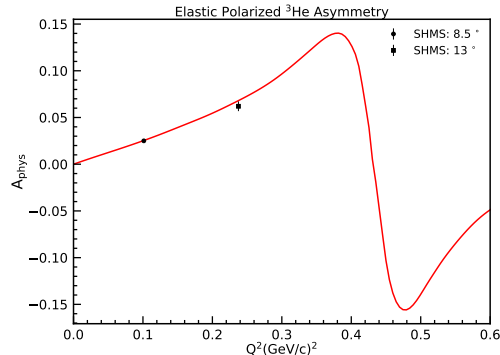


FIG. 1. Measured elastic asymmetry for the  $Q^2 = 0.1$  and  $Q^2 = 0.2$  ( $\text{GeV}/c$ )<sup>2</sup> (red solid circle), along with a prediction for the asymmetry (red curve). The error bar includes both statistical and systematic uncertainties

where  $d_{El}$  and  $A_{El}$  are the fractional contribution from and the asymmetry of elastic scattering. The extracted QE asymmetry was studied further as a function of the excitation energy of  $^3\text{He}$ , defined as

$$E_x = \sqrt{M^2 + 2M\omega - Q^2} - M, \quad (7)$$

where  $M$  is the mass of  $^3\text{He}$  and  $\omega$  is the energy transfer. The two-body and three-body breakups correspond to excitation energies of 5.5 and 7.7 MeV, respectively. Results for the asymmetry are given in Tables I and II, along with both statistical and systematic uncertainties. The systematic uncertainties include contributions from elastic radiative tail subtraction, spectrometer acceptance, and beam & target polarization ( $P_b P_t$ ). The results are compared with three theoretical predictions in Fig. 2.

TABLE I. The measured asymmetry as a function of the excitation energy for  $Q^2=0.1$  ( $\text{GeV}/c$ )<sup>2</sup>.

$E_x$ (MeV)	$A$	$\delta_{stat}$	$\delta_{syst}$
8.0	0.0181	0.0027	0.0013
13.0	0.0114	0.0016	0.0008
18.0	0.0073	0.0016	0.0005
23.0	0.0040	0.0015	0.0003
28.0	0.0038	0.0020	0.0003
33.0	0.0051	0.0019	0.0004
38.0	0.0033	0.0018	0.0002
43.0	0.0026	0.0030	0.0002

Of the three models, one is the relativistic plane-wave impulse approximation [2] that evaluates the spectral function utilizing the AV18 nucleon-nucleon potential [20], along with a Coulomb potential and takes the Höhler parameterization [21] for the form factors. PWIA is generally not expected to be reliable in the three-nucleon system at low energies where rescattering and FSI are

TABLE II. The measured asymmetry as a function of the excitation energy for  $Q^2=0.2$  (GeV/c) $^2$ .

$E_x$ (MeV)	$A$	$\delta_{stat}$	$\delta_{syst}$
8.0	0.0404	0.0023	0.0029
13.0	0.0266	0.0025	0.0019
18.0	0.0128	0.0019	0.0009
23.0	0.0090	0.0018	0.0006
28.0	0.0014	0.0015	0.0001
33.0	0.0057	0.0013	0.0004
38.0	0.0042	0.0012	0.0003
43.0	0.0086	0.0010	0.0006

important. The two remaining models [5, 7] are based on the nonrelativistic Faddeev theory for three-particle scattering and include both FSI and MEC. They differ in the choice of the nuclear interaction, i.e., the AV18 potential with the Urbana IX 3NF was used in the calculations by Golak *et al.* [6] while the CD Bonn +  $\Delta$  potential including an explicit  $\Delta$ -isobar excitation and the proton-proton Coulomb force was used in the calculations by Deltuva *et al.* [7, 8]. Both Faddeev calculations utilized electromagnetic form factors from Hammer *et al.* [22]. As can be seen in Figure 2, both nonrelativistic Faddeev calculations have an overall good agreement with data at both kinematics, while PWIA fails at lower excitation energies. This finding is consistent with a previous study at low  $Q^2$ , where the Faddeev calculations could explain the experimental data [11] considerably better than PWIA.

We report here a recent, precision measurement of the double-spin asymmetry in electron quasielastic scattering off a  $^3\text{He}$  target. The asymmetries are presented as functions of the excitation energy and are compared with theoretical calculations using PWIA and Faddeev equations with two different nucleon-nucleon potential inputs. Both Faddeev-based calculations agree with the new data fairly well, though the PWIA agrees with data only at high excitation energies. We expect that the new data set, taken at relatively low energy and momentum transfer, will be confronted with incoming predictions based on 2N and 3N potentials as well as electromagnetic current operators derived consistently within chiral effective field theory.

## ACKNOWLEDGMENTS

We thank the Accelerator Division and Hall C technical staff for their support. This material is based

upon work supported in part by the U.S. Department of Energy, Office of Science, Office of Nuclear Physics under contract numbers DE-AC05-06OR23177 (JLab), DE-FG02-99ER41101 (Univ. of Kentucky), and DE-SC0014434 (U. of Virginia). The work of J. Golak, R. Skibiński, and H. Witała (Kraków group) was supported by the Excellence Initiative - Research University

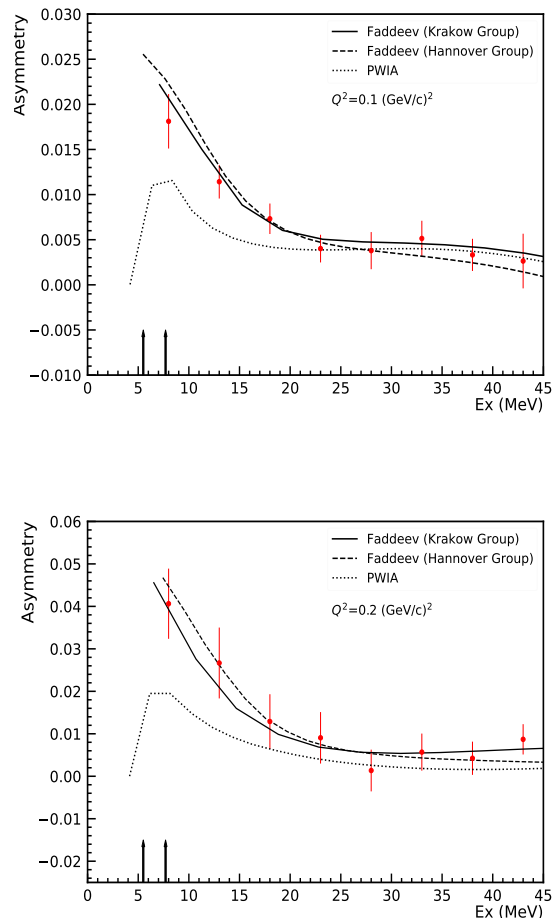


FIG. 2. Results on quasielastic asymmetry for  $Q^2=0.1$  and  $Q^2=0.2$  (GeV/c) $^2$ , along with the theoretical predictions.

Program at the Jagiellonian University in Kraków. The numerical calculations of the Kraków group were partly performed on the supercomputers of the JSC, Jülich, Germany.

[1] M. Mihovilović *et al.*, Physics Letters B **788**, 117 (2019).  
 [2] C. Ciofi degli Atti, E. Pace, and G. Salmè, Phys. Rev. C **1**, 10.1103/PhysRevC.51.1108 (1995).

[3] A. Kievsky, E. Pace, G. Salmè, and M. Viviani, Phys. Rev. C **56**, 64 (1997).  
 [4] E. Pace, G. Salmè, S. Scopetta, and A. Kievsky, Phys.

- Rev. C **64**, 055203 (2001).
- [5] J. Golak, H. Wital, H. Kamada, D. Hüber, S. Ishikawa, and W. Glöckle, Phys. Rev. C **52**, 1216 (1995).
- [6] J. Golak, R. Skibiński, H. Witała, W. Glöckle, A. Nogga, and H. Kamada, Physics Reports **415**, 89 (2005).
- [7] A. Deltuva, L. P. Yuan, J. Adam, and P. U. Sauer, Phys. Rev. C **70**, 034004 (2004).
- [8] A. Deltuva, Physics Letters B **835**, 137552 (2022).
- [9] H. Witała, J. Golak, and R. Skibiński, (2023), arXiv:2310.03433 [nucl-th].
- [10] G. A. Retzlaff *et al.*, Phys. Rev. C **49**, 1263 (1994).
- [11] F. Xiong *et al.*, Phys. Rev. Lett. **87**, 242501 (2001).
- [12] T. W. Donnelly and A. S. Raskin, Annals of Physics (1986).
- [13] S. L. S. Barcus, D. Higinbotham *et al.*, Measurement of  $^3\text{He}$  elastic electromagnetic form factor diffractive minima using polarization observables (2020).
- [14] S. Wood *et al.*, Jefferson Lab Hall C Standard Equipment Manual (2019).
- [15] T. G. Walker and W. Happer, Reviews of Modern Physics **69**, 629 – 642 (1997).
- [16] J. T. Singh, P. A. M. Dolph, W. A. Tobias, T. D. Averett, A. Kelleher, K. E. Mooney, V. V. Nelyubin, Y. Wang, Y. Zheng, and G. D. Cates, Phys. Rev. C **91**, 055205 (2015).
- [17] Hall C SHMS Single Arm Monte Carlo, [https://github.com/JeffersonLab/mc\\_shms\\_single](https://github.com/JeffersonLab/mc_shms_single) (2021).
- [18] S. Barcus, Ph.D. thesis, College of William & Mary (2019).
- [19] A. Amroun *et al.*, Nuclear Physics A **579**, 596 (1994).
- [20] R. B. Wiringa, V. G. J. Stoks, and R. Schiavilla, Phys. Rev. C **51**, 38 (1995).
- [21] G. Höhler, E. Pietarinen, I. Sabba-Stefanescu, F. Borkowski, G. Simon, V. Walther, and R. Wendling, Nuclear Physics B **114**, 505 (1976).
- [22] H.-W. Hammer and U.-G. Meißner, Eur. Phys. J. A **20**, 469–473 (2004) **20**, 469 (2004).